Nanomaterial safety for microbially-colonized hosts: Microbiota-mediated physisorption interactions and particle-specific toxicity

Brinkmann, B.W.

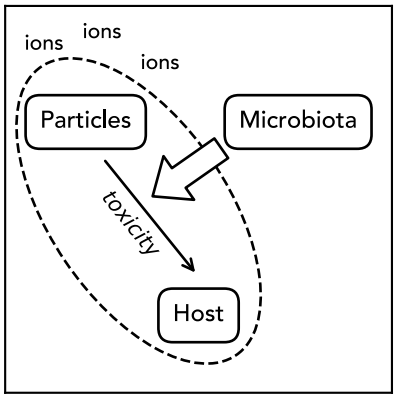
ions
ions
ions
Particles
Microbiota
toxicity
Host

CHAPTER 4

Colonizing microbiota protect zebrafish larvae against silver nanoparticle toxicity

Bregje W. Brinkmann

Bjørn E. V. Koch

Herman P. Spaink

Willie J. G. M. Peijnenburg

Martina G. Vijver

Published in *Nanotoxicology*, 14(6): 725-739 (2020). DOI: 10.1080/17435390.2020.1755469

Data is available via *Figshare*. DOI: 10.6084/m9.figshare.c.4923261

Abstract

Metal-based nanoparticles exhibiting antimicrobial activity are of emerging concern to human and environmental health. In addition to their direct adverse effects to plants and animals, indirect effects resulting from disruption of beneficial host-microbiota interactions may contribute to the toxicity of these particles. To explore this hypothesis, we compared the acute toxicity of silver and zinc oxide nanoparticles (nAg and nZnO) to zebrafish larvae that were either germ-free or colonized by microbiota. Over two days of exposure, germ-free zebrafish larvae were more sensitive to nAg than microbially-colonized larvae, whereas silver ion toxicity did not differ between germ-free and colonized larvae. Using response addition modeling, we confirmed that the protective effect of colonizing microbiota against nAg toxicity was particle-specific. Nearly all mortality among germ-free larvae occurred within the first day of exposure. In contrast, mortality among colonized larvae increased gradually over both exposure days. Concurrent with this gradual increase in mortality was a marked reduction in the numbers of live host-associated microbes, suggesting that bactericidal effects of nAg on protective microbes resulted in increased mortality among colonized larvae over time. No difference in sensitivity between germ-free and colonized larvae was observed for nZnO, which dissolved rapidly in the exposure medium. At sublethal concentrations, these particles moreover did not exert detectable bactericidal effects on larvae-associated microbes. Altogether, our study shows the importance of taking host-microbe interactions into account in assessing toxic effects of nanoparticles to microbially-colonized hosts, and provides a method to screen for microbiota interference with nanomaterial toxicity.

Keywords: Fish Embryo Acute Toxicity Test; Host-microbiota interactions; Particle-specific toxicity; Gnotobiotic techniques; Germ-free.

4.1 Introduction

Microbiota that reside in and on plants and animals, interact closely with their hosts, modulating immune responses, nutrient uptake and energy metabolism (Hacquard et al. 2015; Brugman et al. 2018). Healthy hosts with beneficial microbiota harbor diverse mutualistic and commensal microbes, yet restrict growth of pathogenic microbes. Perturbation of the interactions between hosts and interacting microbiota, called 'dysbiosis', has been related to severe infections, metabolic disorders and immune diseases across humans, animals and plants (Willing et al. 2011). For this reason, the release of antimicrobial agents into the environment, potentially disturbing host-associated microbiota, raises concerns about human and environmental health (Adamovsky et al. 2018; Trevelline et al. 2019).

Of emerging concern are metal-based nanoparticles that appear as new antimicrobial agents on the market (Seil and Webster 2012). Examples of antimicrobial nanoparticles include silver, zinc oxide, titanium dioxide, copper and iron oxide particles. These metal nanoparticles can disrupt and damage cellular membranes, DNA and proteins, either as a result of their physical interaction with these cellular components, or by inducing the formation of reactive oxygen species (Bondarenko et al. 2013; Brandelli et al. 2017). Additionally, metal nanoparticles release toxic metal ions, either in- or outside of cells, that exert similar adverse effects (Seil and Webster 2012; Brandelli et al. 2017). Notably, nanoparticles and their shed ions do not only affect microbial cells, but can also exert adverse effects on plants and animals (Yang et al. 2017b; Sukhanova et al. 2018).

Whilst at risk of the negative consequences of dysbiosis, some microbes can interact with antimicrobial nanoparticles, potentially reducing the nanoparticles' toxicity to the host. *In vitro* studies, for instance, have demonstrated that several bacteria can reduce toxic silver ions back into their less toxic particulate form (Lin et al. 2014). Moreover, experiments in micro- and mesocosm setups revealed that microbiota can enhance their production of extracellular polysaccharides in response to chronic nanoparticle exposure (Eduok and Coulon 2017). By trapping antimicrobial nanoparticles, extracellular polysaccharides presumably offer protection against toxic nanoparticles. Whether such interactions occur among host-associated microbiota *in vivo*, and whether these interactions significantly affect the toxicity of nanoparticles to the host, is still unknown. Nevertheless, human gut microbiota have already been found to affect the toxicity of other environmental pollutants, either bioactivating or detoxifying compounds such as (nitro-)polycylic aromatic hydrocarbons, nitrotoluenes, polychlorobiphenyls, metals, and benzene derivatives (Claus et al. 2016).

In recent years, zebrafish larvae have proven to be a useful model organism to study host-microbiota interactions *in vivo* (Rawls et al. 2004; Meijer et al. 2014). Zebrafish larvae also continue to be an important model organism in toxicology for both human and environmental hazard assessment (Bambino and Chu 2017; Horzmann and Freeman 2018). Similar to embryos of other teleost fish species, zebrafish embryos are assumed to develop in a sterile environment inside of the chorion, until they hatch at 2 days post-fertilization (dpf). Then, microbes that densely colonize the outer surface of chorions, and microbes from the surrounding water, likely colonize zebrafish larvae externally. Quickly thereafter, zebrafish open their mouth (at 3 dpf) and start feeding (at 5 dpf), allowing microbial colonization of their gastrointestinal tracts (Llewellyn et al. 2014). Based on this colonization cycle, Rawls et al. (2004) established gnotobiotic techniques that enable quick and easy derivation of zebrafish larvae that are either germ-free or colonized by specific microbes or microbiota.

In this study, we combined gnotobiotic techniques for zebrafish larvae with standardized toxicity tests (Fish Embryo Acute Toxicity Test, OECD Test No. 236) enabling to explore the impact of host-associated microbiota on the acute toxicity of silver and zinc oxide nanoparticles (nAg and nZnO). Specifically, we investigated 1) how colonizing microbiota affect the sensitivity of zebrafish larvae to nAg and nZnO; 2) to what extent these impacts of microbiota-host interactions relate to the particle-specific toxicity of nAg and nZnO, rather than to the toxicity of their shed Ag^{+} and Zn^{2+} ions; and 3) how nAg and nZnO affect the abundance and the composition of colonizing microbiota. To this end, we compared the acute toxicity of nAg and nZnO between germ-free and microbially-colonized zebrafish larvae. Using response addition modeling, we derived the relative contribution of nanoparticles and their shed ions to the toxicity of nanoparticle suspensions. At the end of the exposures, we isolated bacteria from zebrafish larvae, and counted their abundance as an estimation of microbiota quantity. Finally, we identified the isolated colony-forming units based on 16S rRNA gene sequencing, to reveal what bacterial species associating with zebrafish larvae are potentially resilient to nanoparticle toxicity.

4.2 Materials and methods

4.2.1 Nanoparticle dispersions

Silver nanoparticles (nAg) with a primary particle size of 15 nm (NM-300K; Klein et al. 2011) were kindly provided by RAS AG (Regensburg, Germany). These particles are commercially available as an aqueous suspension (agpure® W10) comprising 10% (w/w) Ag nanoparticles, 4% ammonium nitrate, 4% (w/w) polyoxyethylene glycerol trioleate, and 4% (w/w) polyoxyethylene sorbitan mono-laurat. Uncoated zinc oxide

nanoparticles (nZnO) with a primary particle size of 42 nm (NM-110) (Singh et al. 2011) were purchased from the Joint Research Centre (Ispra, Italy) of the European Union (EU).

Immediately prior to exposure, stock suspensions of both nanoparticles were prepared in egg water (60 mg·L^{-1} Instant Ocean sea salts; Sera GmbH, Heinsberg, Germany) at a final concentration of 100 mg·L^{-1}. According to the batch dispersion protocol of the EAHC NANOGENOTOX project (v.1; Jensen 2018b), nAg was handled in an argon atmosphere to prevent particle oxidation. Stock suspensions were stabilized by sonication for 10 min in an ultrasonic water bath (USC200T; VWR, Amsterdam, The Netherlands). The acoustic power of the sonicator was 12 W, as determined following the sonicator calibration standard operation procedure delivered in the EU FP7 NANoREG project (v. 1.1; Jensen et al. 2018). The stock solutions were diluted to the appropriate test concentrations in egg water.

The size and morphology of both nanoparticles were characterized by transmission electron microscopy. To this end, dispersions of 10 mg·L^{-1} nAg and nZnO were prepared in egg water as described above. Five µL of these dispersions were transferred onto 200 mesh carbon-coated copper transmission electron microscopy grids (Ted Pella, Redding, California). The grids were dried at room temperature in the dark for at least 24 h. Particles on the grids were imaged with a 100 kV JEOL (Tokyo, Japan) 1010 transmission electron microscope at 50k-60k times magnification. The size of 50 particles from TEM images of nAg and nZnO was measured using ImageJ software (v. 1.51h; Abramoff et al. 2004).

The hydrodynamic size and zeta potential of nAg and nZnO aggregates were determined using a Zetasizer Ultra instrument (Malvern Panalytical, Malvern, United Kingdom) following 0, 2, 4, 6 and 24 h of exposure (section 4.2.3). We applied the standard operation procedure (SOP) delivered in NANoREG (v. 1.1; Jensen 2018a), but used a fixed number of 10 runs and 3 repeated measurements per sample (n=3). We selected the Smoluchowski formula for approximation of zeta potentials from electrophoretic mobility. For nAg, the refractive index (R_i) and absorption value (R_{abs}) were set to 0.180 and 0.010 respectively, in accordance with Bove et al. (2017). For nZnO, R_i and R_{abs} were set to 2.02 and 0.40 respectively, following the aforementioned SOP. Exposure concentrations below 1.5 mg nAg·L^{-1}, and below 10 mg nZnO·L^{-1} are omitted, as high variation between repeated measurements (SEM > 30% of the mean hydrodynamic size) and high polydispersity indices (≥0.70), indicate that the concentration of aggregates in these samples was too low for accurate dynamic light scattering analyses.

4.2.2 Zebrafish larvae and colonizing microbiota

Embryos and larvae of AB×TL wild-type zebrafish were used for all experiments. Adult zebrafish were kept at 28 °C in a 14 h:10 h light:dark-cycle. Zebrafish husbandry and handling were in compliance with local and European animal welfare regulations (EU Animal Protection Directive 2010/63/EU), as surveyed by the Animal Welfare Body of Leiden University. Standard protocols (https://zfin.org) were used for the maintenance and handling of zebrafish adults and their larvae.

We divided fertilized embryos over two groups:

1. Embryos of the first group were raised according to standard protocols (https://zfin.org). It is assumed that larvae of this group are colonized by microbes from the surrounding water and from chorions, directly upon hatching (Llewellyn et al. 2014).
2. Embryos of the second group were sterilized and raised in autoclaved egg water, in order to exclude any microbial colonization. We sterilized these embryos using the 'Natural breeding method' described by Pham et al. (2008), with the adaptations made by Koch et al. (2018). We further adapted the protocol by Koch et al. (2018) by using half of the concentration of sodium hypochlorite recommended, to ensure that all embryos hatched naturally. Briefly, embryos were incubated from 0-6 hours post fertilization (hpf) in antibiotic- and antimycotic-containing egg water (100 $\mu g \cdot mL^{-1}$ Ampicillin, 5 $\mu g \cdot mL^{-1}$ Kanamycin, 250 $ng \cdot mL^{-1}$ Amphothericin B). From these, 150 embryos were collected in 15 mL conical tubes at 6 hpf. Under sterile conditions, the embryos were washed with 3 mL 0.2% PVP-iodine in egg water for 45-60 s and rinsed twice with 10 mL sterile egg water. Thereafter, the embryos were washed twice with 6 mL 0.03% sodium hypochlorite (3.5% Cl_2; VWR International, Radnor, PA) in egg water for 5 min. Embryos were rinsed once with 10 mL sterile egg water in between these washing steps, and were rinsed thrice with 10 mL sterile egg water following both sodium hypochlorite washing steps. Only if we could not isolate any bacterial colonies from the resulting larvae on solid LB growth medium, as described in section 4.2.5, larvae were included in this germ-free group.

As a control for the sterilization treatment, embryos of a third group were first sterilized as described for group 2, and were recolonized immediately thereafter by placing the embryos in egg water of the non-sterilized group 1. However, in agreement with the principles of ecological succession (Odum 1969), specifically microbes with high growth rates, such as *Pseudomonas aeruginosa,* appeared to recolonize zebrafish embryos following initial sterilization, in favor of microbes with slower growth rates, such as *Phyllobacterium myrsinacearum* and *Sphingomonas leidyi* (Fig. S1). For this reason, we

continued our experiments with embryos of group 1 and 2 only. The embryos of both groups were incubated at 28 °C in petri dishes with 30 mL egg water until the start of exposure.

4.2.3 Exposures

Microbially-colonized and germ-free zebrafish larvae were exposed to nanoparticle dispersions from 3 to 5 dpf in 24-well plates as described by Van Pomeren et al. (2017b). This setup is based on OECD guideline No. 236 (OECD 2013), with the modification of exposing 10 larvae for each test concentration together in one well, instead of exposing 20 larvae for each test concentration in separate wells. This modification reduces the total amount nanomaterial that is required per test, and produces similarly robust data to the original test (Van Pomeren et al. 2017b). Three biological replicates were tested for each nominal test concentration. These were 0, 0.25, 0.75, 1, 1.5 and 2.5 mg nAg·L^{-1}, and 0, 2.5, 5, 8, 10 and 20 mg nZnO·L^{-1}. Additionally, to test the impacts of potentially shed ions, zebrafish larvae were exposed to solutions of $AgNO_3$ and $Zn(NO_3)_2$ in egg water. The nominal test concentrations to derive dose-response curves for these salt solutions were 0, 0.025, 0.05, 0.1, 0.2 and 0.4 mg Ag^+·L^{-1}; and 0, 2.5, 5, 6, 7.5, and 15 mg Zn^{2+}·L^{-1}. Because Ag^+ and Zn^{2+} ions exert antimicrobial activity, the $AgNO_3$ and $Zn(NO_3)_2$ stock solutions can be expected to be sterile. However, since exposure of germ-free zebrafish larvae to microbes can induce a major transcriptional response, resulting in altered leukocyte infiltration in the intestines (Koch et al. 2018), $AgNO_3$ and $Zn(NO_3)_2$ stock solutions were autoclaved for this group out of precaution. Control groups were exposed to egg water without nanoparticles or corresponding salt solutions. Exposure took place in the dark at 28 °C. After 24 h of exposure, dead embryos were removed, and nanoparticles and salt solutions were refreshed. Mortality was scored following 24 h and 48 h of exposure.

The above setup is based on two assumptions, which we tested. Firstly, we assumed that mortality in nAg exposures resulted either directly from the particles, or indirectly from their shed ions, but was not caused by the dispersion medium itself. In order to verify this assumption, particles from a 100 mg·L^{-1} stock dispersion of nAg were spun down thrice at 20 000 × *g* for 30 min, and zebrafish larvae were exposed to the autoclaved supernatant following the above setup. Secondly, we assumed that the iodine and sodium hypochlorite rinsing steps that are part of the sterilization protocol, do not alter the dissolution of particles. To test this assumption, we compared particle dissolution in microbially-colonized and germ-free exposures as described in section 4.2.4.

4.2.4 Derivation of particle-specific toxicity

Actual concentrations of nanoparticles and their shed ions were determined using atomic adsorption spectrometry. At 0 h and 24 h following the start of exposure, 3-5 mL of the nanoparticle dispersions at each test concentration were sampled to determine total metal concentrations (n=3). Another 4 mL of each nanoparticle dispersion was centrifuged for 30 min at 20 000 × g, and 3 mL of the supernatant was sampled to determine metal ion concentrations (n=3). The samples were acidified with 0.5% HCl and 1% HNO_3, and were stored in the dark until further analysis. Elemental concentrations of Zn and Ag in the acidified samples were measured using an Analyst 100 flame atomic absorption spectrometer (Perkin Elmer, Waltham, Massachusetts). Elemental particle concentrations were calculated by subtracting ion metal concentrations from total metal concentrations. In a few cases for nZnO, where particle concentrations were below the detection limit (as indicated by <D.L.), this calculation produced negative values, which we set to zero. Particulate and total ZnO concentrations were derived from the elemental Zn concentrations based on differences in molar mass. Subsequently, replicate measurements were averaged, and the time weighted average concentration (C_{TWA}) was calculated for ions, particles and total metals, as proposed for nanosafety research by Zhai et al. (2016):

$$C_{TWA} = \frac{c_{t=0h} + c_{t=24\,h}}{2} \qquad \text{(eq 4.1)}$$

where $c_{t=0h}$ is the average concentration at 0 h, and $c_{t=24h}$ is the average concentration at 24 h following the start of exposure. Finally, the mean particle-specific contribution to mortality ($\overline{E_{particle}}$) was determined for each nanoparticle test concentration by way of response addition (Bliss 1939):

$$\overline{E_{total}} = 1 - [(1 - \overline{E_{ion}})(1 - \overline{E_{particle}})] \qquad \text{(eq 4.2)}$$

where $\overline{E_{total}}$ corresponds to the mean mortality in nanoparticle exposures at the total CTWA, and $\overline{E_{ion}}$ corresponds to the mean mortality in $AgNO_3$ and $Zn(NO_3)_2$ exposures at the ion CTWA. The standard deviation of $\overline{E_{particle}}$ was derived by propagating the standard deviation of $\overline{E_{total}}$ following:

$$\sigma_{\overline{E_{particle}}} = \overline{E_{particle}} \sqrt{\left(\frac{\sigma_{\overline{E_{total}}}}{\overline{E_{total}}}\right)^2} \qquad \text{(eq 4.3)}$$

where $\sigma_{\overline{E_{particle}}}$ and $\sigma_{\overline{E_{total}}}$ represent the standard deviations of $\overline{E_{particle}}$ and $\overline{E_{total}}$.

4.2.5 Microbiota colony-forming units

Microbiota were isolated from zebrafish larvae at 5 dpf using a tissue homogenizer. To this end, 3 larvae were transferred to a 1.5 mL SafeLock microcentrifuge tube (Eppendorf, Nijmegen, the Netherlands) comprising 200 µL autoclaved egg water and 6 zirconium oxide beads (1.0 mm-diameter; Next Advance, New York, New York). The larvae were anaesthetized for 2 min on ice, homogenized for 15 s in a tissue homogenizer (Bullet Blender model Blue-CE; Next Advance) at speed 7, and cooled for 10 s on ice immediately thereafter. The homogenization and cooling steps were repeated 7 times to obtain a total homogenization time of 2 min.

As a measure of microbiota abundance, we determined the number of colony-forming units (CFUs) associated with larvae from the lowest exposure concentrations and controls at the end of exposures. Microbes were isolated from zebrafish larvae as described in section 4.2.5, using 3 instead of 5 larvae per microcentrifuge tube. Isolated microbiota were diluted in autoclaved egg water (10, 100 and 1000 times) to reach appropriate CFU densities, and 100 µL of the diluted microbiota was plated on LB agarose. Undiluted isolates from germ-free larvae were also plated (100 µL). Following 2 days of incubation at 28 °C, CFUs were counted. We continued the incubation at 28 °C for 3 additional days, to check if any new colonies appeared. If colonies appeared in the germ-free group, data from the corresponding larvae were excluded from the experiment. Dilutions with the highest countable number of CFUs below 200 were used to estimate microbiota abundances. It should be noted that we used our CFU estimates as a relative rather than absolute measure of microbiota abundance. Many bacteria can still not be cultured, and will thus not grow on LB growth medium. Moreover, we showed that our isolation method is detrimental to a small fraction of the isolated bacteria as presented in the Supplementary Fig. S2.

Thirty colonies of nAg-exposed larvae and their controls were selected for 16S rRNA-based bacterial identification (60 colonies in total). Individual colonies were freshly grown on solid LB growth medium overnight at 28 °C, and a swap of each colony was lysed for 3 min in 100 µL nuclease free water at 100 °C. Of these, a 1505-nt fragment of the 16S rRNA gene was amplified in polymerase chain reactions (PCR) with 27F (5'-AGAGTTTGATCMTGGCTCAG-3') and 1492R (5'-TACGGYTACCTTGTTACGACTT-3') universal bacterial primers (Lane 1991). The PCR reactions had a total volume of 50 µL and contained 1 µL colony lysate, 5 µL 10× PCR buffer (200 mM Tris-HCl pH 8.4, 500 mM KCl), 5 µL dNTP mix (2mM), 1 µL $MgCl_2$ (50 mM), 0.5 µL of each primer (100 µM) and 0.5 µL Taq DNA polymerase (5 $U \cdot \mu L^{-1}$) in nuclease free water. The reactions were performed with an initial denaturation step of 5 min at 94 °C, followed by 30 cycles of denaturation (30 s at 94 °C), annealing (30 s at 58°C), and extension (30 s at 72 °C), and a final extension step of

10 min at 72 °C. The DNA sequence of PCR products was determined by BaseClear, Leiden by way of Sanger sequencing with 27F primers. We trimmed low-quality areas of the obtained sequence chromatograms, and corrected chromatograms manually where necessary using 4Peaks software (by A. Griekspoor and Tom Groothuis; nucleobytes.com). For each of the resulting sequences, we performed a BLASTn search against NCBI's nucleotide database (https://blast.ncbi.nlm.nih.gov/) to identify the corresponding species.

4.2.6 Statistical analyses

All statistical analyses were performed in R (v. 3.4.0; www.r-project.org). Results are reported as mean ± standard error of the mean (SEM), calculated using the 'bear' package (v. 2.8.3; pkpd.kmu.edu.tw/bear). All figures were plotted using Python (v. 3.6.5) with the 'numpy' (v. 1.15.0), 'matplotlib' (v. 2.2.2) and 'pandas' (v. 0.23.3) packages.

In order to investigate particle dissolution, mean nanoparticle concentrations at 0 h and 24 h following exposure were compared for each of the five exposure concentrations in a two-way ANOVA design without interaction between exposure concentration and exposure time. The mean concentrations of shed ions at 0 h and 24 h were compared in a similar model. Subsequently, to test if the sterilization procedure affected nAg dissolution, we compared mean nAg and Ag^+ concentrations between exposure wells with microbially-colonized and germ-free larvae using a Welch Two Sample t-test (for nAg) and Two Sample t-test (for Ag^+) respectively. Diagnostic plots were inspected to verify if the model assumptions were met. Additionally, the Shapiro-Wilk test for normality was performed to check if residuals of the ANOVA and t-tests followed a normal distribution. We performed an F test to compare two variances to check if the variance was equally distributed over the microbially-colonized and germ-free groups.

For dose-response analyses, mortality data were fitted to a three-parameter log-logistic model using the *drm* function of the 'drc' package (v. 3.0-1; Ritz et al. 2005). The lower limit of the models was set to 0, and slope, inflection point (LC_{50}) and upper limit were estimated. LC_{50} estimates were compared between colonized and germ-free larvae using the *compParm* function. We obtained mortality estimates (mean and SEM) from ion (Ag^+/Zn^{2+}) and nanoparticle (nAg/nZnO) dose-response curves, at the measured ion C_{TWA} and total C_{TWA} respectively, by interpolation using the *predict* function. From these mortality estimates, we derived particle-specific mortality estimates (mean and SEM) by way of response addition as described before (section 4.2.4). We used these mean and SEM particle-specific mortality estimates to simulate particle-specific

mortality data at each of the exposure concentrations (n=3) using the *rnorm* function of the stats package (v. 3.5.1). Finally, we fitted a three-parameter log-logistic function to these particle-specific mortality data and particle C_{TWA} estimates, and compared particle-specific LC_{50} estimates of germ-free and colonized larvae using the *compParm* function.

The CFU counts of control larvae, and larvae that were exposed to the lowest exposure concentrations of nAg, Ag^{+}, nZnO and Zn^{2+}, were compared using an ANOVA test, combined with Tukey's HSD post-hoc test. For this model, log(x+1) transformation of CFU counts was required to ensure that the residuals of the model followed a normal distribution, as indicated by the Q-Q plot and Shapiro-Wilk test for normality. We used the diagnostic plots of the model to check for equal variance of residuals across larvae of the control, nAg, Ag^{+}, nZnO and Zn^{2+} exposures.

4.3 Results

4.3.1 Nanoparticle size, shape, aggregation and dissolution

Dispersions of nAg comprised spherically shaped primary particles with a diameter ranging from 8 nm to 42 nm (average 24 nm; n=50; Fig. 4.1). Following dispersion in the exposure medium, the particles formed aggregates with mean hydrodynamic sizes of 218 ± 109 nm and 140 ± 59 nm at nominal exposure concentrations of 1.5 mg nAg·L^{-1} and 2.5 mg nAg·L^{-1}, respectively. The size of nAg aggregates remained similar over the first 6 h of incubation, and reached a mean hydrodynamic size of 67 ± 7 nm at 24 h of incubation (Fig. S3a), the time at which the exposure medium was replaced. Accordingly, the mean zeta potential of aggregates remained around -20 mV over 24 h of incubation, indicating that particles remained stable over the incubation time (Fig. S3b).

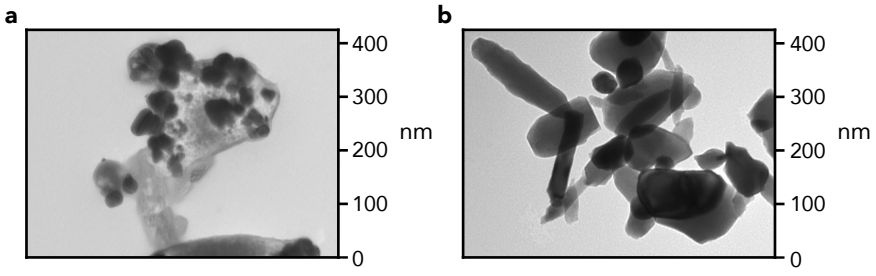

Figure 4.1: *Transmission electron microscope images of nAg and nZnO particles* at 60k and 50k magnification respectively.

Primary particles of nZnO had irregular shapes, with a width ranging from 12 nm to 109 nm (average 47 nm; n=50), and a length ranging from 17 nm up to 234 nm (average 94 nm; n=50; Fig. 4.1). At nominal exposure concentrations of 10 and 20 mg nZnO·L^{-1}, these primary particles formed aggregates with hydrodynamic sizes of 1086 ± 326 nm and 822 ± 193 nm at the start of incubation, and 806 ± 176 nm and 423 ± 73 nm at 24 h of incubation, respectively (Fig. S3c). The corresponding zeta potential measurements indicated that nZnO aggregates stabilized over the first 2 h of incubation, reaching a zeta potential of around -30 mV (Fig. S3d).

Immediately following dispersion, nAg and nZnO released ions into the exposure medium (Fig. 4.2a,c). No ions could be detected in controls without particles. Following 24 h of incubation, mean concentrations of Ag^+ ions in the exposure medium were still similar to those at the start of exposures (Fig. 4.2a,b; Table S1; $F_{1,24}$= 0.025, p>0.05). We note that this result needs to be interpreted with caution, as the assumption of normally distributed model residuals was not met, even following log or rank transformation. In accordance with the similar concentrations of Ag^+ ions measured at 0 h and 24 h of incubation, we could not detect any differences between mean mass-based particle concentrations at 0 h and 24 h of incubation for nAg (Fig. 4.2a,b; Table S1; $F_{1,24}$=1.1, p>0.05). Furthermore, the sterilization procedure to obtain germ-free larvae, including rinsing steps with sodium hypochlorite and PVP-iodine, did not result in higher concentrations of Ag^+, or lower concentrations of nAg, in the exposure medium (Table S2). In contrast to Ag^+, mean concentrations of Zn^{2+} were significantly higher following 24 h of incubation than at the start of exposures (Fig. 4.2c,d; Table S1; $F_{1,24}$= 26.9, p=2.6·10^{-5}). The dissolution of nZnO appeared to be concentration-dependent, where the release of Zn^{2+} seemed to have saturated already at the start of exposure at nominal concentrations below 8 mg ZnO·L^{-1}, whereas concentrations of Zn^{2+} in the exposure medium increased over 24 h of exposure at nominal concentrations above 8 mg ZnO·L^{-1}. Despite this release of ions, we did not detect differences between mass-based nZnO concentrations between 0 h and 24 h of incubation in the exposure medium (Fig. 4.2c,d; Table S1; $F_{1,24}$= 0.26, p>0.05).

4.3.2 Impact of microbiota on nanoparticle toxicity

Zebrafish larvae that were colonized by microbes responded differently to dispersions of nAg than germ-free zebrafish larvae (Fig. 4.3a). Following 48 h of exposure, median lethal toxic concentrations (LC_{50}) were significantly higher for microbially-colonized larvae (LC_{50}= 0.94 ± 0.14 mg Ag·L^{-1}), than for germ-free larvae (LC_{50}= 0.34 ± 0.06 mg Ag·L^{-1}; p=0.0006; Fig. 4.3a). Mortality among microbially-colonized larvae increased from 24 h to 48 h of exposure. In contrast, nearly all mortality among germ-free larvae

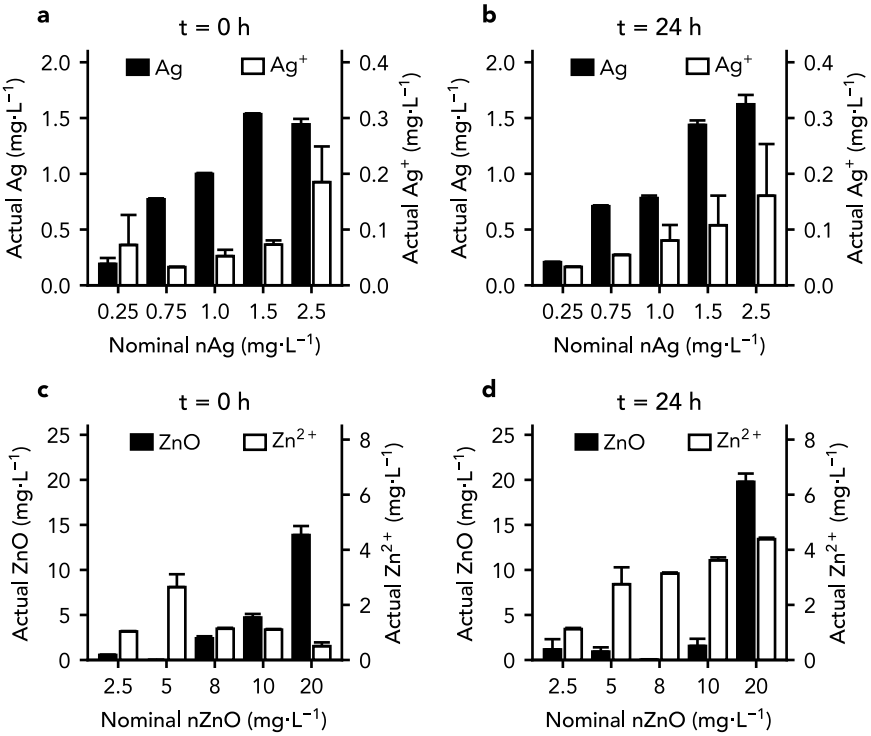

Figure 4.2: *Dissolution of nAg* (**a**,**b**) *and nZnO* (**c**,**d**) *nanoparticles*. Bars depict the mean concentrations of particles (black bars, left axis) and their shed ions (white bars, right axis) at 0 h (**a**,**c**) and 24 h (**b**,**d**) following dispersion, for each of the nominal test concentrations. Error bars indicate standard error of the mean (*n*=3). Values are provided in Table S1.

occurred within the first day of exposure. When nAg was removed from the dispersion medium by centrifugation prior to exposure, and larvae were exposed for 48 h to the nAg-dispersion medium without particles, we did not observe any mortality among larvae of each microbiota group.

In contrast to the effects of nAg, median lethal toxic concentrations of Ag^+ did not differ between the microbially-colonized larvae (0.14 ± 0.02 mg $Ag^+ \cdot L^{-1}$) and germ-free larvae (0.16 ± 0.06 mg $Ag^+ \cdot L^{-1}$; p=0.74; Fig. 4.3b) following two days of exposure. However, similar to the results of nAg exposures, nearly all mortality among germ-free larvae occurred during the first day of exposure to Ag^+, while mortality among colonized larvae gradually increased over the two days of exposure.

No differences in median lethal concentrations of nZnO dispersions were observed between germ-free larvae (4.91 ± 0.43 mg ZnO·L^{-1}) and colonized larvae (4.68 ± 0.62 mg ZnO·L^{-1}; p>0.05; Fig. 4.3c) following two days of exposure. Moreover, mortality among both germ-free and colonized larvae increased from 24 h to 48 h of exposure to nZnO.

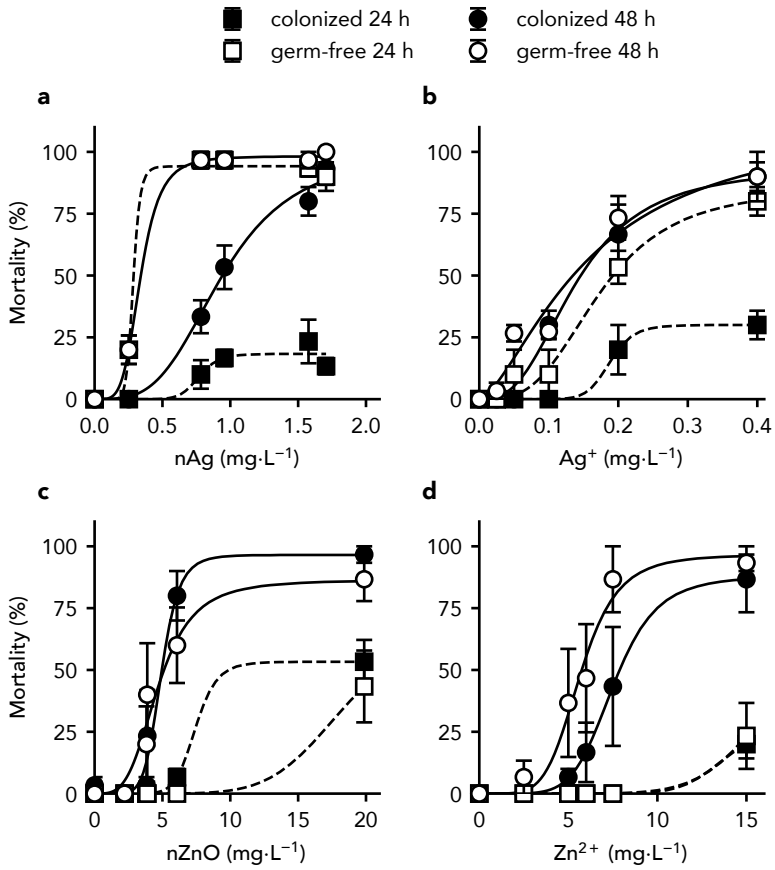

Figure 4.3: *Dose response curves of microbially-colonized* (black markers) *and germ-free* (white markers) *zebrafish larvae* exposed to nAg (**a**), Ag^{+} (**b**), nZnO (**c**), and Zn^{2+} (**d**) following 24 h (squares) and 48 h (circles) of exposure. Error bars depict the standard error of the mean (n=3).

Similar to nZnO, we did not detect differences between median lethal concentrations of Zn^{2+} for colonized larvae (7.54 ± 0.82 mg $Zn^{2+}{\cdot}L^{-1}$) and germ-free larvae (5.68 ± 0.47 mg $Zn^{2+}{\cdot}L^{-1}$; p>0.05; Fig. 4.3d). Furthermore, mortality among Zn^{2+}-exposed larvae increased over the second day of exposure, independent of microbial colonization.

In order to explore the particle-specific contributions to the observed toxicity of nAg and nZnO, dose response curves were corrected for the effects of shed ions in the exposure medium by way of response addition (Fig. 4.4). The particle-specific LC_{50} estimates that were obtained for nAg in this way, still differed significantly between colonized (0.84 ± 0.06 mg particulate $Ag{\cdot}L^{-1}$) and germ-free larvae (0.34 ± 0.20 mg particulate $Ag{\cdot}L^{-1}$; t=2.35, df=4, p=0.03). At median lethal concentrations of total silver,

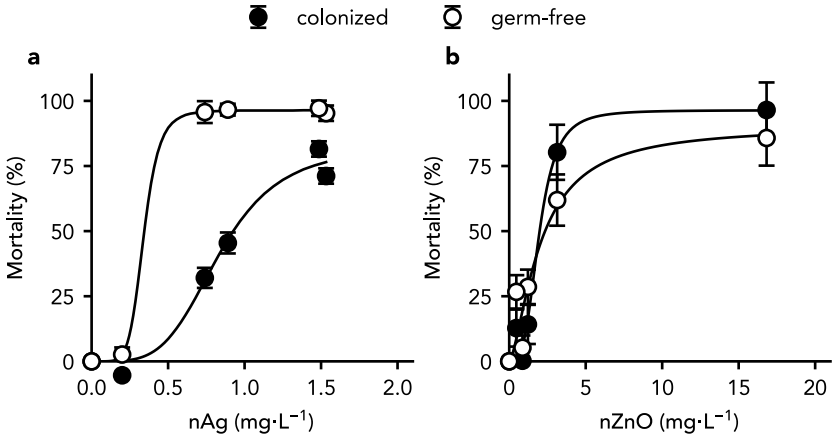

Figure 4.4: *Particle-specific dose response curves of microbially-colonized* (black markers) *and germ-free* (white markers) *zebrafish larvae* exposed to nAg (**a**), and nZnO (**b**) following 48 h of exposure. Error bars depict the standard error of the mean (*n*=3).

93 ± 13 % and 42 ± 57 % of the mean mortality under colonized and germ-free conditions respectively, could be explained by the particle-specific contribution to toxicity. For nZnO, particle-specific median lethal toxic concentrations did not differ between microbially-colonized conditions (1.94 ± 0.25 mg particulate $ZnO \cdot L^{-1}$) and germ-free conditions (2.04 ± 0.48 mg particulate $ZnO \cdot L^{-1}$; t= -0.17, df=4, $p>0.05$). Despite the quick dissolution of these particles, the relative contribution of nZnO particles accounted 97 ± 396 % and 88 ± 431 % of the mean total observed mortality at median lethal concentrations for colonized and germ-free larvae respectively.

4.3.3 Impact of nanoparticles on microbiota

In order to investigate the impacts of nAg and nZnO on zebrafish microbiota, we isolated colony-forming units (CFUs) from zebrafish larvae of the colonized group. At the end of the exposure time, $8.4 \cdot 10^3 \pm 3.6 \cdot 10^3$ CFUs per larvae could be isolated from the control group (Fig. 4.5). Exposure to the lowest test concentrations of nAg (0.25 $mg \cdot L^{-1}$), Ag^+ (0.025 $mg \cdot L^{-1}$), nZnO (2.5 $mg \cdot L^{-1}$), and Zn^{2+} (2.5 $mg \cdot L^{-1}$) affected this CFU count ($F_{4,10} = 45.5$, $p=2.2 \cdot 10^{-6}$; Fig. 4.5). Fewer CFUs could be isolated from larvae that were exposed to nAg (0.89 ± 0.59 CFUs per larvae; $p=0.00002$) and Ag^+ ($1.3 \cdot 10^2 \pm 1.1 \cdot 10^2$ CFUs per larvae; $p=0.001$). Exposure to nZnO or Zn^{2+} did not result in different CFU counts per larvae, as compared to control larvae ($p>0.05$).

Considering the bactericidal effects of nAg, we further explored what bacterial species remained among the isolated CFUs following exposure to nAg, selecting 30 CFU

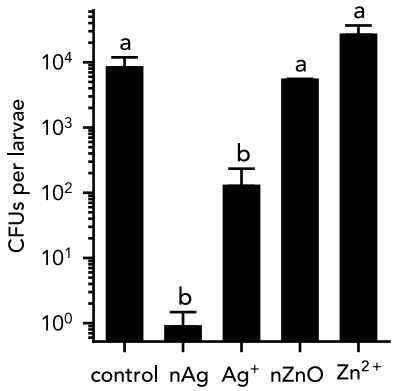

Figure 4.5: *Number of colony-forming units (CFUs) associated with zebrafish larvae* at the lowest exposure concentrations of nAg (0.25 mg·L^{-1}), Ag^+ (0.025 mg·L^{-1}), nZnO (2.5 mg·L^{-1}) and Zn^{2+} (2.5 mg·L^{-1}). Bars depict the mean CFU count per larvae (n=3), error bars depict the standard error of the mean, and letters indicate significant differences (p<0.05).

isolates of nAg-exposed larvae and 30 CFU isolates of control larvae for 16S rRNA gene-based identification. In total, we identified 52 of 60 selected bacteria with >98% sequence identity (Table S3). The other 8 CFUs had low sequence quality, resulting in 16S rRNA identity <98%. Nevertheless, BLAST results suggested similar bacterial species for these CFUs, as for the CFUs with >98% sequence identity. Hence, these records were included in the sequence identities presented below.

Based on 16S rRNA sequence identity, we identified 6 different bacterial species among isolated CFUs (Fig. 4.6). Additionally, we identified 3 groups of bacteria that we could not distinguish based on 16S rRNA sequences. Most of the isolated CFUs corresponded to *Phyllobacterium myrsinacearum* (30%), followed by bacteria of the genus *Pseudomonas* (30%; 13% of which was *P. aeruginosa*), *Delftia lacustris/D. tsuruhatensis* (17%), *Rhizobium rhizoryzae* (17%), and *Sphingomonas leidyi* (7%). Exposure to nAg and Ag^+ changed the relative abundance of these bacteria among isolated CFUs. The relative abundance of *P. myrsinacearum* was higher (63%) among CFUs of exposed larvae compared to non-exposed larvae. Additionally, we identified several bacterial species that did not appear among selected CFUs of non-exposed larvae, including *Bosea* sp. (13%), bacteria of the genus *Microbacterium* (17%), and *Staphylococcus* bacteria/*Sulfitobacter donghicola* (7%).

4.4 Discussion

Multicellular organisms live in association with diverse microbiota that contribute to host health and development. The emergence of metal-based nanoparticles on the

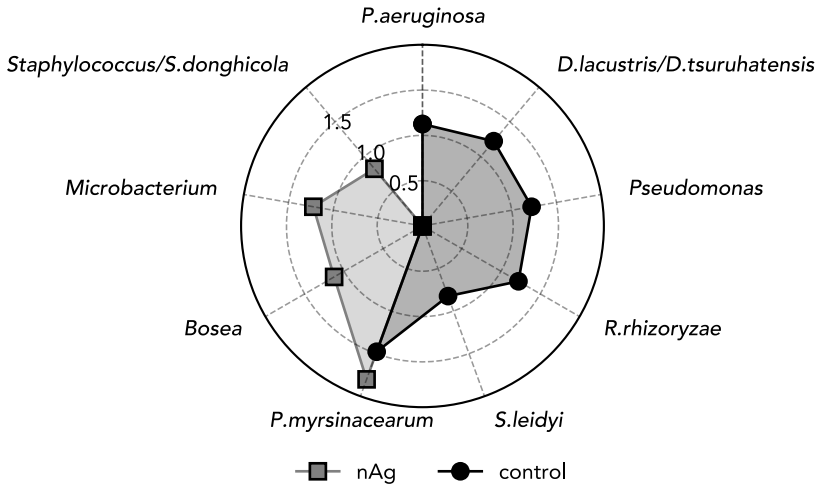

Figure 4.6: *Impacts of nAg* (0.25 mg·L^{-1}) *on the composition of colony-forming units (CFUs) isolated from zebrafish larvae* (30 colonies each). Radial axes depict $\log_{10}$-transformed relative abundances (%) of bacterial species. The corresponding BLAST results are included in Table S3. *Abbreviations*: *D. lacustris/D. tsuruhatensis*, *Delftia lacustris/Delftia tsuruhatensis*; *P. aeruginosa*, *Pseudomonas aeruginosa*; *P. myrsinacearum*, *Phyllobacterium myrsinacearum*; *R. rhizoryzae*, *Rhizobium rhizoryzae*; *S. donghicola*, *Sulfitobacter donghicola*; *S. leidyi*, *Sphingomonas leidyi*.

market poses a threat to these host-associated microbiota, owing to the inherent antimicrobial properties of these particles. Ultimately, nanoparticle-induced perturbation of host-associated microbiota might affect both human and environment health (Adamovsky et al. 2018; Trevelline et al. 2019). For this reason, we set out to explore the role of zebrafish larvae-associated microbiota in the acute toxicity of the two commonly applied antimicrobial nanoparticles nAg and nZnO, explicitly quantifying the relative contributions of particles and shed ions to toxicity.

4.4.1 Protection of host-associated microbiota against nanoparticles

By combining standardized acute toxicity tests and established gnotobiotic techniques, we found that colonizing microbiota protect zebrafish larvae against particle-specific lethal effects of nAg, increasing the LC_{50} from 0.34 ± 0.20 mg particulate Ag·L^{-1} under germ-free conditions to 0.84 ± 0.06 mg particulate Ag·L^{-1} under microbially-colonized conditions. Following two-days of exposure, we did not detect this microbially-mediated protection against Ag^+, observing similar LC_{50} values for microbially-colonized and germ-free larvae. This suggests that interactions between microbes and particles, rather than interactions between microbes and particle-shed ions, underlie the protective effect of microbiota. We also did not observe any differences between the

sensitivity of germ-free and colonized larvae to nZnO and Zn^{2+}. This similar sensitivity of germ-free and colonized larvae to nZnO and Zn^{2+} indicates that the protective effect against nAg results from specific interactions between microbes and particles, rather than general differences in health between germ-free and colonized larvae.

It is still unclear what mechanisms underlie the microbially-mediated protection against nAg. Notably, the majority of zebrafish larvae that died from nAg exposure under germ-free conditions, already died within the first day of exposure, whereas mortality under microbially-colonized conditions gradually increased over the two days of exposure. Given this acute mortality under germ-free conditions, it is possible that nAg induces an intense pro-inflammatory immune response in zebrafish larvae, which results in increased acute mortality under germ-free conditions. Diverse metal nanoparticles, including silver, copper and gold nanoparticles, have already been found to induce an acute immune response in zebrafish larvae (Brun et al. 2018; Poon et al. 2019; Van Pomeren et al. 2019). Moreover, Poon et al. (2019) found that nAg, but not nZnO, induces inflammatory immune responses in THP-1 cells. In case immune responses underly the differences in sensitivity between germ-free and colonized conditions, the absence of immune responses in response to nZnO might explain why we did not observe differences in sensitivity between germ-free and colonized larvae to nZnO. Interestingly, Koch et al. (2018) have shown that colonizing microbiota can suppress immune responses in zebrafish larvae via Myd88 signaling. Combined, these findings suggest that colonizing microbiota could protect zebrafish larvae against nAg, by suppressing pro-inflammatory immune responses that are induced by these particles.

4.4.2 Effects of nanoparticles on host-associated microbiota

Concurrent to the mortality among zebrafish larvae, nAg and Ag^{+} killed the majority of zebrafish larvae-associated microbes, with barely any culturable microbes remaining after two days of exposure to nAg. Similarly high bactericidal activity of nAg has been demonstrated *in vitro*, with 4-h EC_{50} values based on growth inhibition ranging from 0.35 to 18.7 mg $Ag{\cdot}L^{-1}$ for gram-negative bacteria (including several *Pseudomonas* species, *Bacillus subtilis* and *Escherichia coli*), and 46.1 mg $Ag{\cdot}L^{-1}$ for the gram-positive bacterium *Staphylococcus aureus* (Bondarenko et al. 2013). In contrast, exposure of zebrafish larvae to sublethal concentrations of nZnO and Zn^{2+} did not result in a lower abundance of isolated microbes. Accordingly, *in vitro* studies have shown that zinc oxide particularly exhibits antimicrobial activity against Gram-positive bacteria, whilst the majority our isolates from zebrafish larvae were Gram-negative bacteria (Seil and Webster 2012). Moreover, the lowest concentrations of nZnO that reduced viability of the Gram-positive bacterium *S. aureus* and the Gram-negative bacterium *Escherichia*

coli, as determined in 24 h-*in vitro* exposures (> 400 mg ZnO·L^{-1}; Nair et al. 2009), were well above the sublethal concentration of nZnO applied in our study (2.5 mg ZnO·L^{-1}). This could imply that nZnO and Zn^{2+} did not exert any bactericidal activity against the bacterial isolates of our study. Alternatively, growth of resistant bacteria might have compensated for the loss of affected bacteria.

Considering the bactericidal effects of nAg, we further investigated the effects of these particles on microbiota composition. Without exposure to nAg, CFU isolates included the opportunistic pathogenic bacteria *P. aeruginosa, D. lacustris* and/or *D. tsuruhatensis,* and *S. maltophilia* (Preiswerk et al. 2011; Brooke 2012; Shin et al. 2012; Gellatly and Hancock 2013), and possibly *S. epidermis* (Otto 2009). Following exposure to nAg, we did not isolate any of these species anymore from microbially-colonized larvae. It is still unclear whether nAg elicits immune responses that contribute to the loss of opportunistic bacteria. Only one of the bacterial isolates – *P. myrsinacearum* – appeared to be resistant against nAg. Surprisingly, this species was initially isolated from *Ardisia* leaf nodules (Knösel 1984), and is known to be capable of nitrate reduction (Mergaert et al. 2002). Since nitrate-reducing enzymes can reduce Ag^{+} (Lin et al. 2014), it is tempting to hypothesize that *P. myrsinacearum* is resistant to nAg, and protects zebrafish larvae against nAg, by reducing Ag^{+} ions that are released from nAg back into their less toxic particulate form. However, considering other bacterial resistance mechanisms to silver compounds including nAg that have been identified *in vitro* (Silver 2003; Panáček et al. 2018), it remains to be determined what mechanisms drive bacterial resistance to nAg *in vivo*.

4.4.3 General applicability of the test approach

This study, at the interface between toxicology and host-microbe interaction studies, is to the best of our knowledge the first of its kind. We investigate how microbial colonization affects the sensitivity of a vertebrate host to nanoparticle toxicity. In our experimental setup, we include germ-free conditions in nanoparticle toxicity tests, thereby combining multiple stressors using standardized and established techniques that do not require advanced laboratory equipment (OECD 2013; Pham et al. 2018). We note that this multi-stressor research design can be applied to detect effects of nanoparticles at concentrations below the lowest-observed-effect concentrations in conventional toxicity tests. More specifically, it can be used to screen for the interaction of host-associated microbiota with the toxicity of nanoparticles and other compounds of interest. Although zebrafish that are raised in the laboratory harbor different microbiota as compared to zebrafish in their natural habitats, core groups of their microbiota are strikingly similar (Roeselers et al. 2011). Moreover, despite differences in

microbiota composition, hosts respond to their associated microbiota in conserved ways (Rawls et al. 2016). This supports the use of our laboratory approach to include the role of host-associated microbiota in human and environmental toxicology. Similar opportunities have been established to derive germ-free *Daphnia magna* water fleas (Sison-Mangus et al. 2015; Callens et al. 2016; Manakul et al. 2017), extending these possibilities to include the role of invertebrate microbiota in toxicological research.

Our results imply that longer-term exposure to bactericidal concentrations of nanoparticles might increase the susceptibility of the host to nAg over time due to the loss of protective microbiota. This insight can serve as an early warning for potential chronic toxic effects of nanoparticles. Nevertheless, chronic effects of nanoparticles depend on many variables and thus remain hard to predict. Some bacteria, for instance, may gain resistance against nAg, and the effects thereof are still unknown. The opportunistic pathogens *P. aeruginosa* and *Escherichia coli* have already been found to be able protect themselves against nAg by producing adhesive proteins that enhance nanoparticle aggregation (Panáček et al. 2018). In case such opportunistic pathogens thrive following nAg-exposure *in vivo*, they might cause infections. Although the complete understanding of the effects of long-term exposure to nAg is beyond the scope of this study, the finding in our study, of a profound impact of colonizing microbiota on silver nanoparticle toxicity, contributes to a better understanding of potential effects of antimicrobial nanoparticles on humans and the environment, and merits further experimental attention.

4.5 Conclusions

In this study, we integrate the disciplines of host-microbiota research and nanotoxicology. By combining gnotobiotic techniques with acute toxicity tests, we showed that host-associated microbiota protect zebrafish larvae against particle-specific toxic effects of silver nanoparticles. This protective effect was lost over time, possibly due to the bactericidal effects of silver particles killing protective microbes. Such indirect adverse effects of nanoparticles, in addition to the direct impacts of nanoparticles on the hosts, can be employed in multi-stressor experimental designs that allow detecting otherwise hidden effects of nanoparticles. The results of our study may also contribute to understanding long-term toxic effects of nanoparticles, since chronic exposure of microbially-colonized organisms to low, yet bactericidal concentrations of nanoparticles may enhance their sensitivity to nanoparticles over time. The observed protective effect of colonizing microbiota against silver nanoparticle toxicity moreover suggests that the effects of silver nanoparticles to humans and to the environment may be more severe following pre-exposure to antimicrobial agents. Hence, our results

highlight the importance of taking microbiota interactions into account in human and environmental hazard assessment of silver nanoparticles.

Data availability statement

Data and supporting material are available via Figshare:
https://doi.org/10.6084/m9.figshare.c.4923261 (data)
https://doi.org/10.6084/m9.figshare.12181941.v1 (supporting material)

Acknowledgement

We thank Wouter Beijk for assistance in the laboratory, Gerda Lamers for help with transmission electron microscopy, Rudo Verweij for supervising atomic adsorption spectrometry measurements and Yujia Zhai for supportive discussions about the project. We are grateful to RAS AG for providing silver nanoparticles. This work was supported by the project PATROLS of European Union's Horizon 2020 research and innovation programme under Grant number 760813.